Colloid Polym Sci 277:174–183 (1999)

ORIGINAL CONTRIBUTION

G. Stakkestad
J. Sjöblom
B. Grung
T. Sigvartsen

Surface chemistry of lanthanum chromite I. Multivariate data modelling of Brunauer-Emmett-Teller surface area by the use of particle size distribution data from photon-correlation spectroscopy measurements

Received: 17 June 1998
Accepted in revised form: 31 August 1998

G. Stakkestad · T. Sigvartsen
Prototech AS, Fantoftveien 38
N-5036 Fantoft, Norway

J. Sjöblom · B. Grung
Department of Chemistry
University of Bergen
N-5007 Bergen, Norway

Abstract Particle size distributions, measured by photon-correlation spectroscopy and Brunauer- Emmett-Teller (BET) surface areas, were determined for several lanthanum chromite powders with different dopants. Principal component analysis (PCA) was used to reveal similarities among the different powders with regard to the input variables particle size, BET surface area, and calcination temperature. Correlation among the variables was also easily revealed by PCA. Partial-least-squares multivariate-response modelling was used to calibrate the BET surface area from particle size data and calcination temperatures. A model explaining 93% of the variance in the data, with good predictive power, was developed. The model revealed that the content of smallest-sized particles and the calcination temperature were important parameters in the prediction of the BET surface area.

Key words Lanthanum chromite powder – Dynamic light scattering – BET – Multivariate data analysis – PCA/PLS

Introduction

The interconnect is a critical component in a planar solid oxide fuel cell (SOFC) since, in addition to acting as the electrical connection between individual cells in series, it must also be gas tight in order to prevent mixing of the fuel and oxidizer. Doped lanthanum chromites exhibit the required phase stability, high electronic conductivity, and low ionic conductivity in both reducing and oxidizing environments making them suitable as interconnects at high temperatures (1000 °C). Additionally, these materials are chemically compatible with the other fuel cell components [1]. Some independent studies reveal, however, that lanthanum chromite expands in a reducing atmosphere [2–5], at oxygen partial pressures well within the effective operating range of an SOFC. Doping with aliovalent B-site additives reduces the lattice expansion significantly [6]. The lanthanum chromite powders that we have chosen to characterize contain the traditional Ca and Sr acceptor dopants, Ni and Zn dopants, and some double dopants (Sr with Ni, Cu, and Mg).

In our previous publications [7, 8] we reported on the electrical conductivity, microstructure, and mechanical properties of Ca- and Sr-doped $LaCrO_3$ interconnects for SOFO. Relative density, secondary phases, and grain boundary layers were found to have an impact on the electrical conductivity and the mechanical strength of these materials.

Production of gas-tight, defect-free interconnects for SOFC is important regarding electrical output and lifetime. Defect-free ceramic composites with fine grain microstructures can be obtained by the processing of colloidal particles [9]. During the mixing, dispersing, forming, and firing steps good colloidal control and hence knowledge of the surface chemistry of the components is important. Sintering of the green body to maximum density depends on the surface free energy available in the powder, and the particle packing efficiency.

Hence, important characterization of the ceramic powders is by the Brunauer-Emmett-Teller (BET) surface area, and by the particle size distribution. Knowledge about the surface properties also gives guidelines

regarding types and amounts of dispersant and/or binder for forming the ceramic green body.

This work focuses on characterization of the surface chemistry and particle size distribution of $LaCrO_3$ powders with different dopants synthesized through alternative routes. BET surface area measurements and photon-correlation spectroscopy (PCS) are used to obtain surface area and particle size distributions, respectively.

By the use of multivariate data analysis the correlation between the BET surface area, the particle size distribution, and the calcination temperature of the different powders is studied.

Multivariate-response modelling is used to model the BET surface area as a function of particle size distribution and calcination temperature. The motivation for doing this is that PCS is a much faster method (approximately 10 min) compared to BET surface area measurements (hours). If we are able to model the surface area from the measured particle size distribution data, we save time and still obtain two important parameters for obtaining the best possible sintering condition.

Materials and methods

Chemicals and powders

The lanthanum chromite powders were obtained from two manufacturers.

Powder A (Pyrox, France), 20% Ca-doped lanthanum chromite ($La_{0.8}Ca_{0.2}CrO_{3-\delta}$), produced by the conventional solid-state reaction method (mixing of oxides and firing at ~1200 °C).

Powder B (Praxair Speciality Ceramics, USA) produced by the combustion spray pyrolysis method. For the B powders we specified the amount and type of dopants.

The characteristics of the lanthanum chromite powders are shown in Table 1.

Table 1 Characteristics of the lanthanum chromite powders: powder A (Pyrox, France) and powder B (PSC, USA)

Powder	Nominal	Synthesis	Sintering aid
A1	$La_{0.8}Ca_{0.2}CrO_{3-\delta}$	Solid-state reaction	Y_2O_3
B1	$La_{0.8}Ca_{0.2}CrO_{3-\delta}$	Spray pyrolysis	
B2	$La_{0.85}Ca_{0.15}CrO_{3-\delta}$	Spray pyrolysis	
B3	$La_{0.8}Sr_{0.2}CrO_{3-\delta}$	Spray pyrolysis	
B4	$LaCr_{0.9}Ni_{0.1}O_{3-\delta}$	Spray pyrolysis	
B5	$LaCr_{0.9}Zn_{0.1}O_{3-\delta}$	Spray pyrolysis	
B6	$La_{0.9}Sr_{0.1}Cr_{0.9}Ni_{0.1}O_{3-\delta}$	Spray pyrolysis	
B7	$La_{0.9}Sr_{0.1}Cr_{0.9}Cu_{0.1}O_{3-\delta}$	Spray pyrolysis	
B8	$La_{0.9}Sr_{0.1}Cr_{0.9}Mg_{0.1}O_{3-\delta}$	Spray pyrolysis	

Photon-correlation spectroscopy

PCS or dynamic light scattering [10, 11] utilizes a laser beam to probe a small volume of a particle suspension. As the particles undergo Brownian motion, interference between scattered light produces a fluctuation in the intensity with time at the detector (photomultiplier). This temporal fluctuation, containing information on the motion of particles, is registered and processed by a digital correlator that yields, in real time, the autocorrelation function. The experimental correlation function gives the diffusion coefficient, D, from which the hydrodynamic diameter, d_h of the particles may be calculated from the Stokes-Einstein equation.

The monomodal method uses a cumulant analysis method [12] to evaluate the signal intensity correlator function. The method gives an average particle size which will only have a meaning in an absolute sense if the sample is really monomodal, i.e. only one peak, and monodisperse, i.e. narrow distribution.

A common method, here called multimodal, used for the analysis of the autocorrelation function is the multiexponential sampling method developed by Ostrowsky et al. [13]. This method does not make any assumption about the shape of the size distribution (i.e. normal, monomodal, bimodal, etc.). The intensity distribution can be calculated directly from the autocorrelation function without knowledge of the optical nature of the particles. The intensity distribution can then be converted to a number distribution using Mie theory by calculating the number of particles that yield the observed intensity in each size class [14]. The refractive index is necessary for this conversion. Often this transformation will not be necessary, as comparison of the intensity distribution will be sufficient.

PCS measurements were performed with a Zetasizer 4, from Malvern UK, equipped with a 256-channel correlator. A 5 mW He-Ne laser (wavelength 632.8 nm) is standard with the Zetasizer 4. The powders were dispersed in water and ultrasonicated for 10 min at room temperature. To eliminate aggregates present in the powders, PCS measurements were performed immediately after the ultrasonication step, at a 90° angle. The powders were analysed by the multimodal method, and the intensity distributions were used for comparison and modelling.

PCS is a rapid method for measuring particles in the submicron region, with simple sample preparation. For particles this small, electron microscopy is the only competing technique, but this is time consuming and the sample preparation is complicated. Furthermore, only small amounts, not necessarily being a representative part of the sample, can be measured. The presence of aggregates and irregular-shaped particles in a system is a limitation of PCS analysis [15]. PCS determines the hydrodynamic size based on the translational motion of

the particles, and is valid only for spherical particles. Irregular particles and aggregates display rotational motion. This rotation can contribute significantly to the decay of the autocorrelation function, the net effect being an underestimation of the measured particle size. The importance of the error introduced depends on the particle size and shape. The powders investigated here were de-agglomerated by ultrasonic treatment. Scanning electron microscopy characterization of the powders has revealed that the particles are non-spherical. When a particle is non-spherical and is larger than the incident wavelength, light scattered from different parts of the same particle interfere to produce an angular dependence of the scattered intensity that is characteristic of a particular particle shape. Multiangle dependence was tested on the powders at angles of 30, 60, 90 and 130°. We observed that the A1 powder seemed to possess multiangle dependence while the B powders had only minor deviations in the particle size distribution at varying analysis angles. In the data analysis we therefore use the particle size distribution data taken at 90°.

Fig. 1 Intensity (histogram) or "cumulative percentage fine than" (CPFT) (■) as a function of particle size (nm) for powders A1, B1, B3 and B6

BET surface area measurements

BET surface area measurements were performed with an ASAP 2010, with N_2 used as the adsorptive gas at Statoil Laboratories (Trondheim, Norway). The temperature was kept at 77.35 K. The BET apparatus determines the total specific surface area from the amount of N_2 adsorbed on the surface.

The principal component analysis (PCA) model

PCA is an exploratory data analysis method [16, 17]. By projecting the measured data onto latent variables that are linear combinations of the measured ones, informative low-dimensional plots can be obtained. These plots display information about the variable and sample correlations. In PCA, the latent variables are called principal components (PCs). The PCs are chosen so as to explain as much of the variation in the data as possible while being orthogonal to each other. For most data, substantial data complexity reduction can be obtained by PCA. Since the number of underlying real factors having a significant influence upon the system is usually low, it is often possible to construct only two or three such "super variables" that contain all the information in the data.

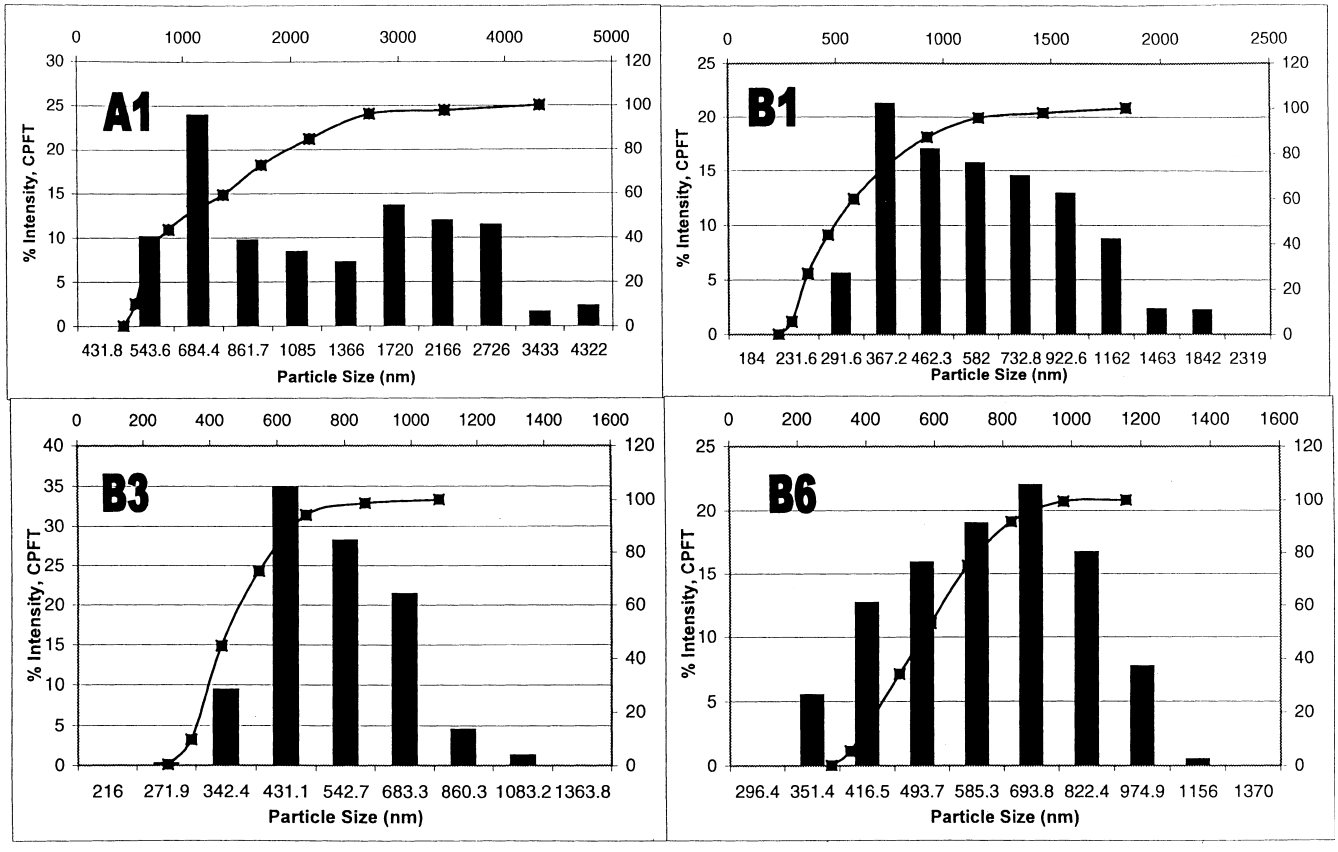

The partial-least-squares (PLS) model

In response modelling, where the covariance between two sets of variables **X** (data matrix) and **Y** (response matrix) is analysed, the principal component is often not the ideal latent variable. The aim is to extract the information in **X** that covaries as much as possible with the information in **Y**. This is done by decomposing the X-room so that the best possible latent variables describe the Y-room. PLS is a much used method for this purpose [18, 19]. PLS decomposes the collinear **X** to a set of uncorrelated latent variables on which the regression coefficient, **b**, is calculated.

Pre-processing of the data

Prior to construction of the PCA and the PLS models, some pre-processing of the data was done in order to have comparable contributions of the different variables to the models. Both the X-block and Y-block matrices were mean-centred and standardized before PCA and PLS algorithms were used. (To standardize a variable means to divide the variable by its standard deviation.)

The data analysis was performed using Sirius for Windows version 1.5 Pattern Recognition System, Norway.

Results and discussion

Particle size

The results from the multimodal particle distribution method are given in Fig. 1 for powders A1, B1, B3, and B6. The intensity as a function of particle size is represented as histograms. The intensity average diameter, d_{50}, and the polydispersity number, which is a dimensionless measure of the broadness of the distribution (see Table 2) can be obtained from the plot.

Particle size distributions of ceramic particles are commonly expressed in terms of "cumulative percentage finer than" (CPFT). In Fig. 1 the CPFT data as function of particle size are also plotted. In Table 2 the parameter used to characterize the particle size, d_x, denotes that x percent has a diameter less than this value when a multimodal analysis method has been used.

Figure 1 and Table 2 reveal that all the powders have broad multimodal particle size distributions (>200 nm width). A1 has a much wider size distribution than the other powders. All the B powders reveal a size distribution that is typical for commercial powders used to manufacture high performance ceramics [20]. The ratio of sizes in the commercial powder is very different from close packed. A higher ratio of coarse/fine-sized particles must then be present in the powders. Several reasons can be taken into account to explain this. First of all, the powders have to be produced relatively cost effectively by industrial techniques such as calcining and milling. Secondly, a higher percentage of small-sized particles is necessary in order to provide a high surface energy (proportional to the surface area) and thus promote easy sintering, even though this discourages close packing. Also, a close packed distribution would not flow readily enough for shaping, since there is not enough empty space for the particles to move between each other easily, even with slight rearrangements; however commercial powder does flow quite easily.

Surface area

Figure 2 shows the adsorption/desorption isotherm for the B1 powder. All powders revealed a similar behaviour upon adsorption and desorption of N_2 gas. According to BET classification of physical adsorption [21], this is a typical type II isotherm. Type II isotherms have a point of inflection at the low-pressure end, and approach the line $P/P_0 = 1$ asymptotically.

Table 2 Particle size (d_x)[a] and polydispersity measured by multimodal photon-correlation spectroscopy, Brunauer-Emmett-Teller (BET) surface area and average pore diameter, calcination temperature and time of the studied powders

Powder	d_{10}	d_{20}	d_{50}	d_{90}	Polydispersity	BET surface area (m^2/g)	Average pore diameter (Å)	Calcination temp (°C)
A1	0.55	0.58	0.97	2.24	0.44	1.76	68.03	1200
B1	0.31	0.33	0.518	1.01	0.31	13.51	112.41	650
B2	0.20	0.22	0.32	0.74	0.32	12.76	120.75	650
B3	0.34	0.37	0.48	0.66	0.17	2.02[b]		1150
B4	0.27	0.29	0.45	1.02	0.36	16.53	146.69	650
B5	0.19	0.21	0.27	0.41	0.26	14.88		650
B6	0.37	0.42	0.50	0.63	0.25	5.71[b]		1000
B7	0.34	0.38	0.54	0.81	0.17	2.72[b]		1000
B8	0.24	0.26	0.51	0.80	0.15	7.21[b]		1000

[a] The parameter used to characterize the particle size, d_x, denotes that x percent has a diameter less than this value
[b] BET surface area measurements performed by Praxair Speciality Ceramics, pore diameter not available

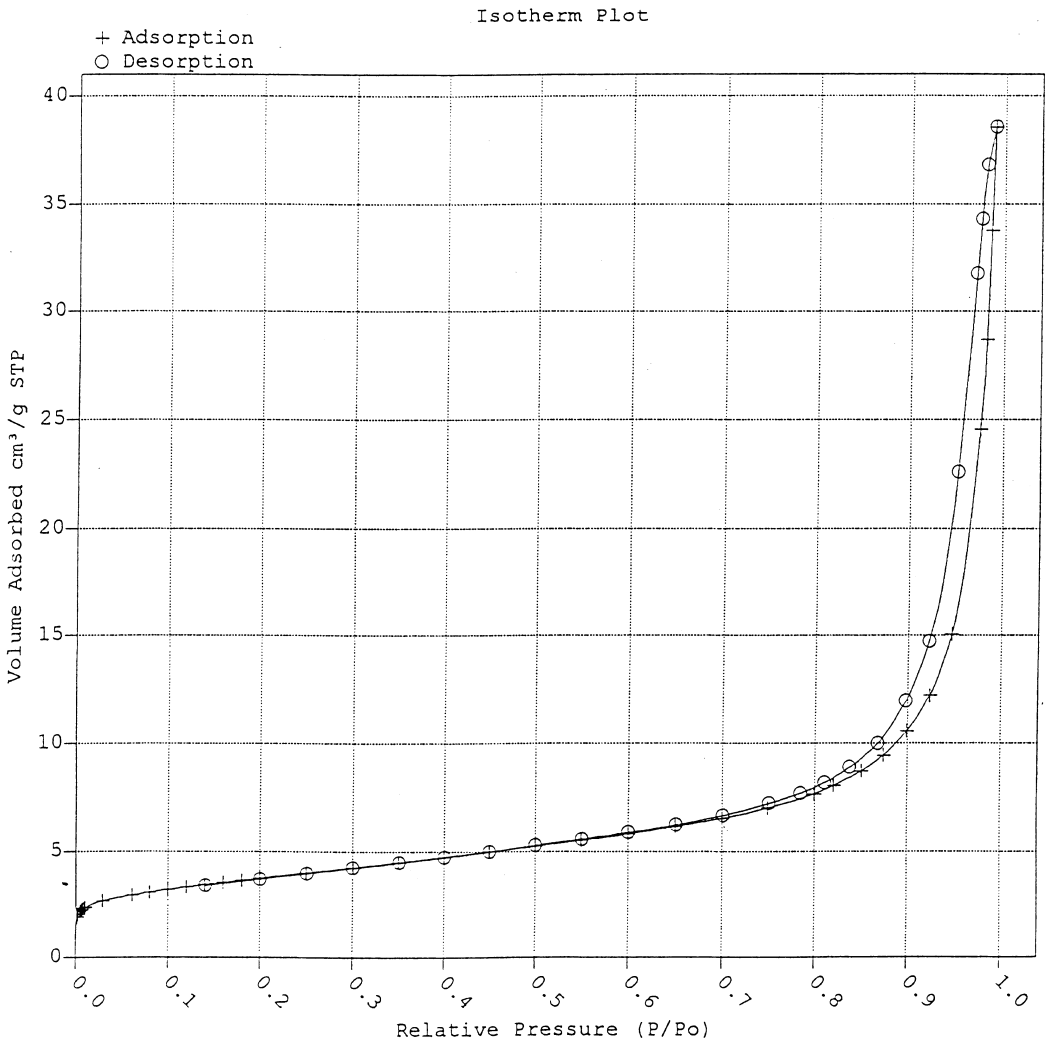

Fig. 2 Adsorption/desorption isotherm plot for powder B1, relative pressure (P/P_0) as a function of N_2 volume adsorbed (cm^3/g) at STP

From this type of isotherm it is possible to calculate the specific surface area, and to make an estimate of the mean pore diameter [22]. The calculated BET surface areas and mean pore diameters for the powders are given in Table 2. Calcination time and temperature are also included. The surface areas of the powders range from 1.8 to 16.5 m^2/g, indicating a significant difference in the surface free energy, and hence, different promotion of sintering. The pore diameter of the powder indicates intermediate pores, as classified in Ref. [23] to be those with diameters between approximately 20 and 200 Å.

Good precursors for ceramics and superconductors have surface areas of about 10 m^2/g [20]. In this case the balance between obtaining a high surface energy for promotion of sintering, and a particle distribution that packs well is often optimal.

Principal component analysis

An explorative PCA was performed with the lanthanum chromite powders as objects and the eight variables from Table 2. The data was standardized and mean-centred prior to the PCA. Two principal components explained 86.4% of the total variance in the data: PC1 explained 64.7%, and PC2 explained 21.7%. This means that a reduction from eight variable space to two-variable space preserves 86.4% of the variance in the data. Figure 3 shows the score plot. The angle and distance between two objects (powders) in the score plot relative to the origin is a measure of their similarity. The powders are distributed into three classes. Class 1 contains powders B1, B2, B4, and B5, while class 2 contains powders B3, B6, B7, and B8. The last powder, A1, differs from the other powders.

The loading plot, Fig. 4, gives an indication of the correlation pattern between the variables. Variables with a small angle in the plot are highly positively correlated.

A 90° angle indicates no correlation, and an angle of 180° reveals that the variables are negatively correlated. We clearly see that BET surface area and calcination temperature are negatively correlated, indicating that when the calcination temperature decreases the surface area increases. This is a well-known result for ceramic powders and has also been observed by others [24–26]. Both BET surface area and pore diameter negatively correlate with the particle diameter. The BET surface area and pore diameter increase when the particle diameter of the powder decreases, which means that powders with high BET surface area values and large pore diameters contains some portion of very fine powder. This correlation has been observed for other oxide ceramic powders [27, 28]. Calcination temperature and particle diameter can be said to positively correlate from this loading plot. When the calcination temperature is increased the powder contains fewer portions of

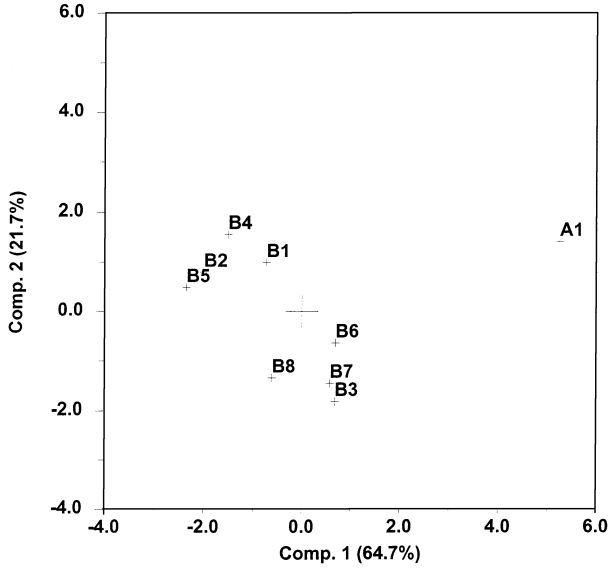

Fig. 3 Score plot from principal component analysis (PCA) of all powders in Table 2. PC1 explains 64.7% of the variance, while PC2 explains 21.7%

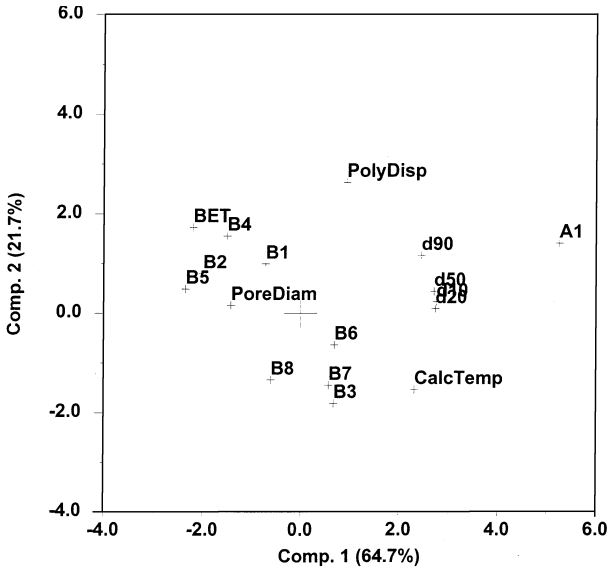

Fig. 5 Biplot from PCA of all powders in Table 2. PC1 explains 64.7% of the variance, while PC2 explains 21.7%

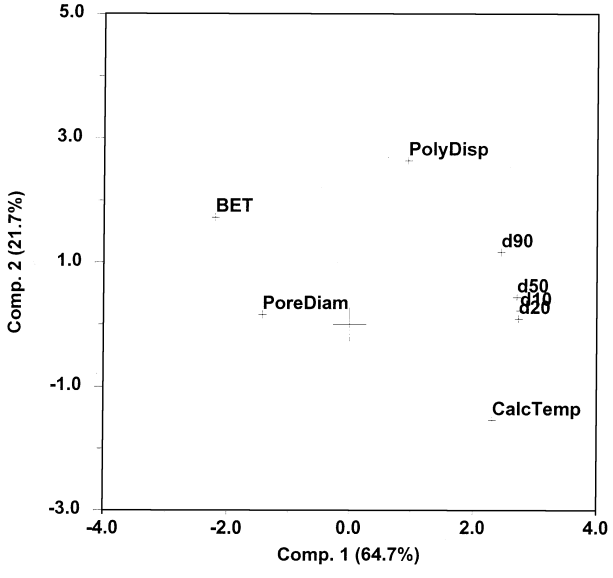

Fig. 4 Loading plot from PCA of all powders in Table 2. PC1 explains 64.7% of the variance, while PC2 explains 21.7%

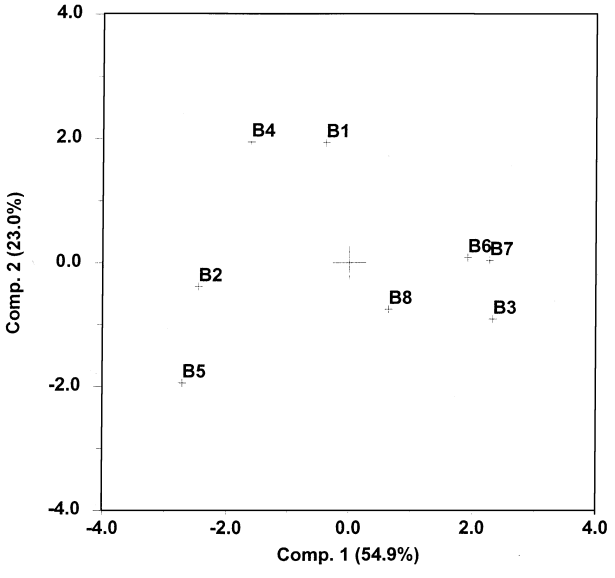

Fig. 6 Score plot from PCA of B powders in Table 2. PC1 explains 54.9% of the variance, while PC2 explains 23.0%

fine particles, which is also a result observed by others [24, 28]. Polydispersity and d_{90} also correlate positively.

We observe the same type of correlation patterns for lanthanum chromite powders as observed for other ceramic powders with regard to the variables studied. The uniqueness of the multivariate PCA decomposing method applied here is that we can study correlation patterns among all variables in one plot. Conventionally variable interactions have only been studied two at a time before.

A combination of the score plot and loading plot, a so-called biplot, Fig. 5, gives information on which variables are related to the different classes. The biplot reveals that class 1 is characterized by large BET surface areas and pore-diameters, and a low calcination temperature. Class 2 is characterized by a high calcination temperature and a low BET surface area value. The object A1, seems to be characterized by a large particle diameter and polydispersity. An alternative way of approaching this is to say that A1 is a typical outlier that does not seem to fit into either of the other two classes. Since A1 is the only powder produced by solid-state reactions, while all the other powders are produced by the spray pyrolysis method, this is a reasonable result.

Since A1 is classified as an outlier, PCA without this powder was also performed. Figure 6 reveals the score plot of this analysis. The total variance explained in this two-component model is 77.9%. The B powders are still distributed into two classes: class 1 contains B1, B2, B4, and B5, while class 2 contains B3, B6, B7, and B8.

A loading plot from the analysis of the B powders is shown in Fig. 7. By excluding A1 we see that the correlation pattern between the variables is altered to some extent. Polydispersity is now more positively correlated to BET surface area. In addition d_{90} has changed from negatively to being positively correlated to BET surface area. The pore diameter does not seem to contribute in this two-component PCA, as it almost coincides with the origin.

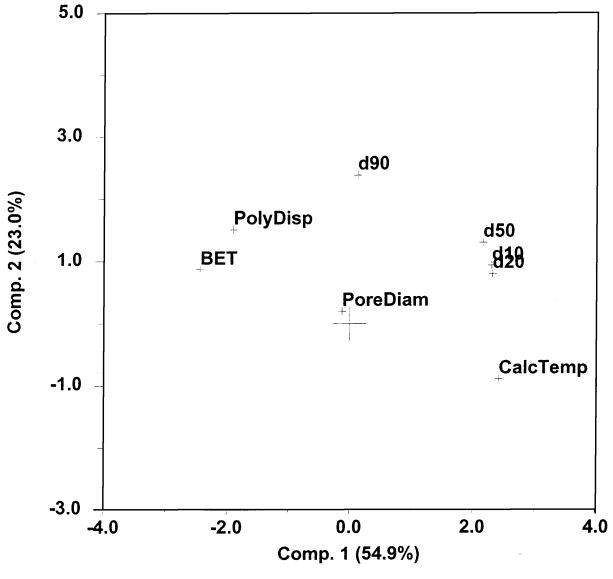

Fig. 7 Loading plot from PCA of B powders in Table 2. PC1 explains 54.9% of the variance, while PC2 explains 23.0%

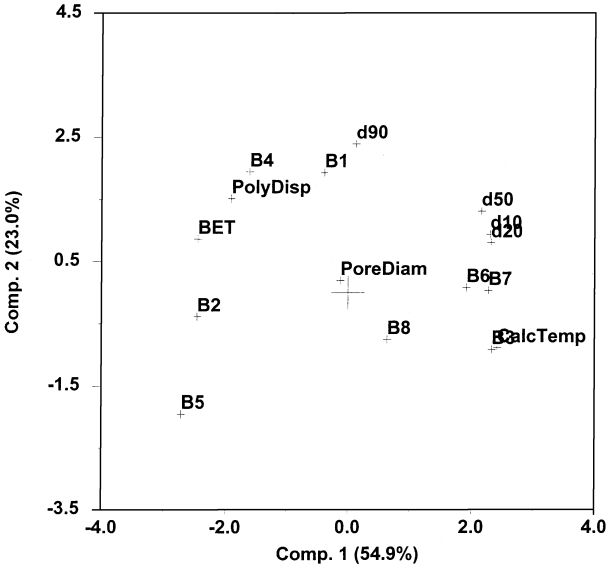

Fig. 8 Biplot from PCA of B powders in Table 2. PC1 explains 54.9% of the variance, while PC2 explains 23.0%

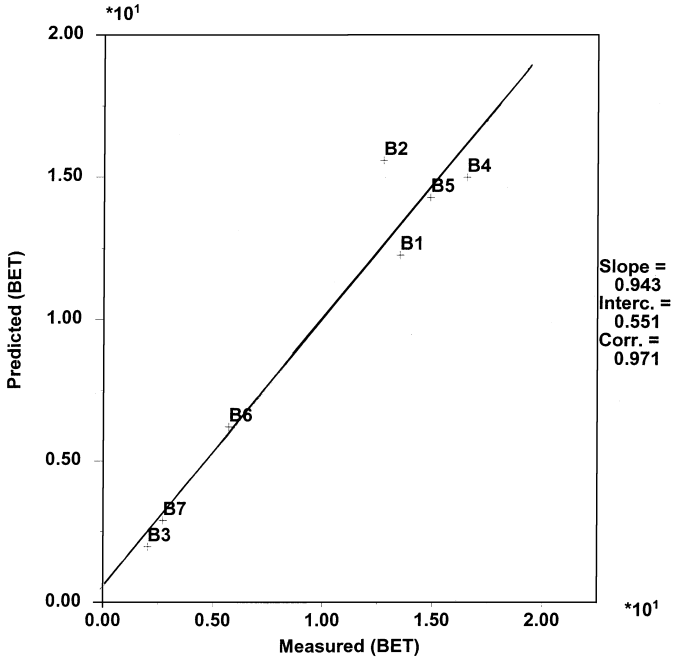

Fig. 9 Predicted vs measured Brunauer-Emmett-Teller (BET) surface area for model 1, all powders, except A1 and B8, and the variables d_{50}, polydispersity, and calcination temperature. Explained variance 97.1%, and a predictive error of 63.2%

A biplot, Fig. 8, reveals that class 1 is characterized by high polydispersity, a large BET surface area, low calcination temperature, and d_{10-50}, while class 2 powders have high calcination temperatures and high d_{10-50} corresponding to low BET surface area values.

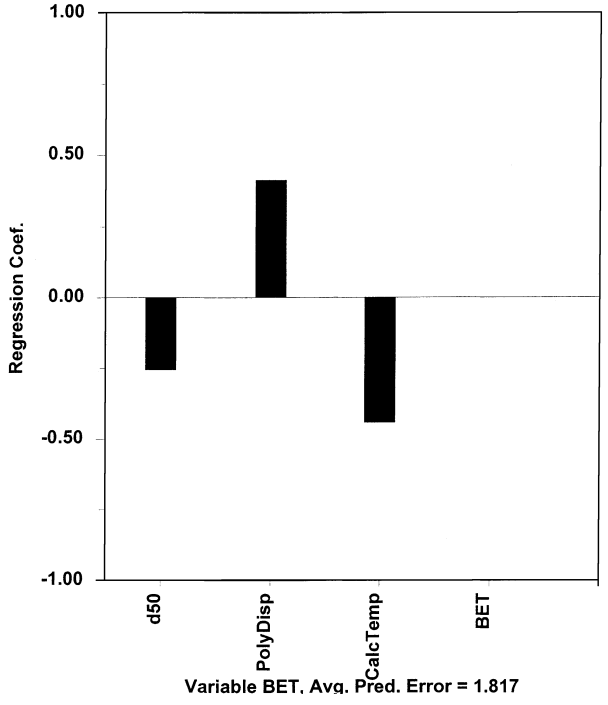

Fig. 10 Regression coefficients for model 1

Multivariate regression

By using multivariate response modelling (PLS) we wanted to check if it was possible to model the specific surface area (BET) from the particle size distribution data and calcination temperature.

In the first PLS model we tried to predict the BET surface area (**Y**-matrix) of the powders in Table 2, except A1 and B8, by the use of the variables d_{50}, polydispersity, calcination temperature, and calcination time (**X**-matrix). A1 was excluded due to its outlying nature. B8 was left out of the modelling so that it could be used as an independent validation sample for the final model. A one-component model explaining 97.1% variance in **Y** was estimated. Figure 9 shows a plot of predicted versus measured surface area for the calibration samples. The regression coefficient plot, Fig. 10, reveals that the two variables that contribute most to the model are the polydispersity and the calcination temperature. The B8 powder has been measured to have a BET surface area of 7.21 m^2/g. By using this one-component model we were able to predict the value of the BET surface area to be 2.65 m^2/g, which means 63.2% predictive error.

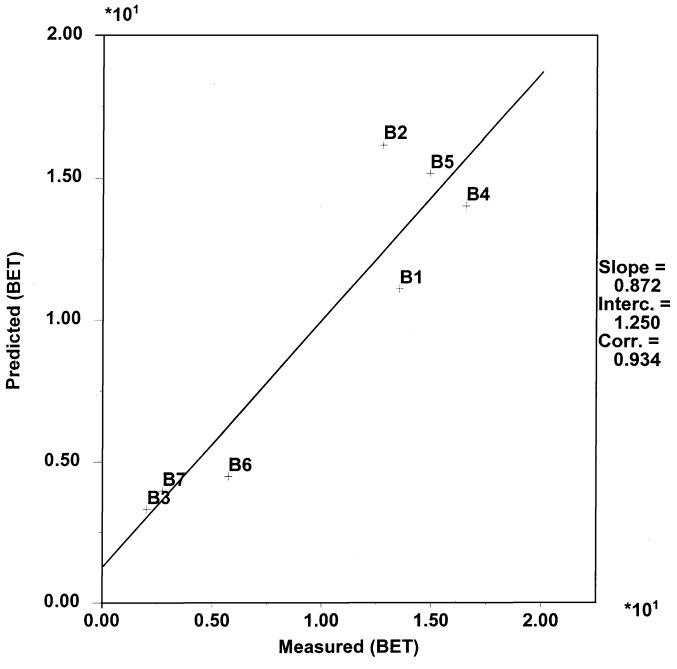

Fig. 11 Predicted vs measured BET surface area for model 2, all powders, except A1 and B8, and the variables d_{10}, d_{20}, d_{50}, d_{90}, polydispersity, and calcination temperature. Explained variance 93.4%, and a predictive error of 1.8%

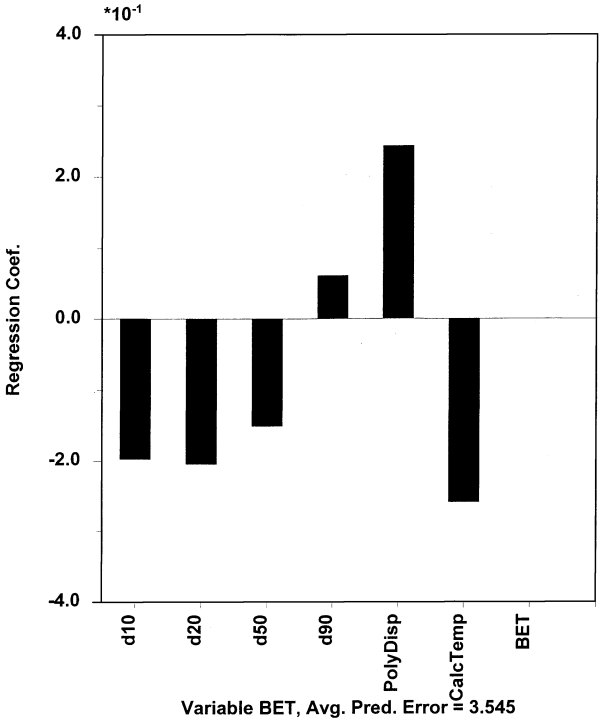

Fig. 12 Regression coefficients for model 2

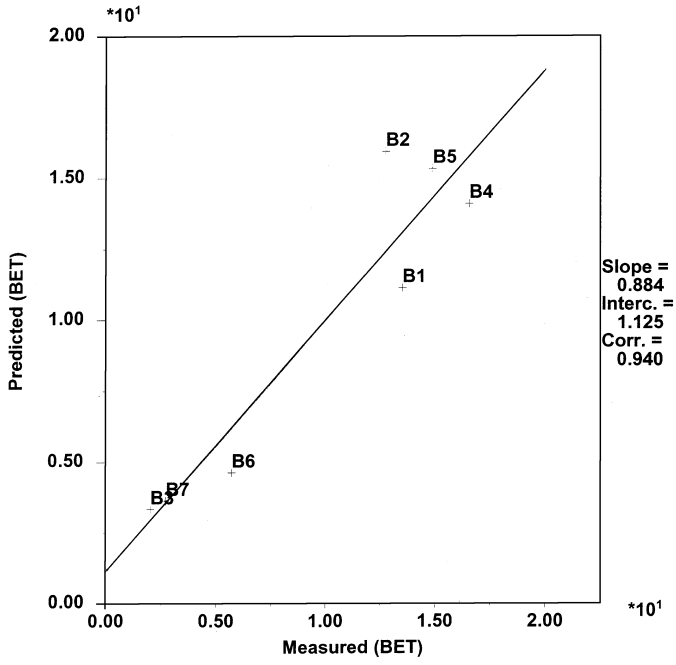

Fig. 13 Predicted vs measured BET surface area for model 3, all powders, except B8, and the variables, d_{10}, d_{20}, d_{50}, d_{90}, polydispersity, calcination temperature, and their cross-terms. Explained variance 94.0%, and a predictive error of 3.2%

By including the variables d_{10}, d_{20}, and d_{90} a second model was extracted. A one-component model explained 93.4% of the variance in **Y** (Fig. 11). The regression coefficient plot, Fig. 12, reveals that d_{10} and d_{20} contribute more to the model than d_{50} and d_{90}. Prediction of the BET surface area value for the B8 powder from this model gives a surface area of 7.34 m^2/g, and the predictive error is reduced to only 1.8%. This verifies the importance of determining the portion of finest particle sizes to be able to estimate the BET surface area.

Further attempts on model improvement were made by including cross-terms of the variables. A one-component model explained 94.0% of the variance in **Y**, Fig. 13. The model predicted the BET surface area of the B8 powder to be 7.44 m^2/g. The predictive error increased to 3.2% when cross-terms were included in the model. Figure 14 shows a normal plot of the regression coefficients where we see that calcination temperature, polydispersity, and their cross-terms contribute to a large extent to the model d_{10} and d_{20} with cross-terms also give good contributions to the model.

PLS modelling/calibration of the BET surface area with the variables in Table 2 gave very good results. We clearly see that the determination of the finest fraction of particles, d_{10} and d_{20}, together with knowledge about the calcination temperature made a great impact on the

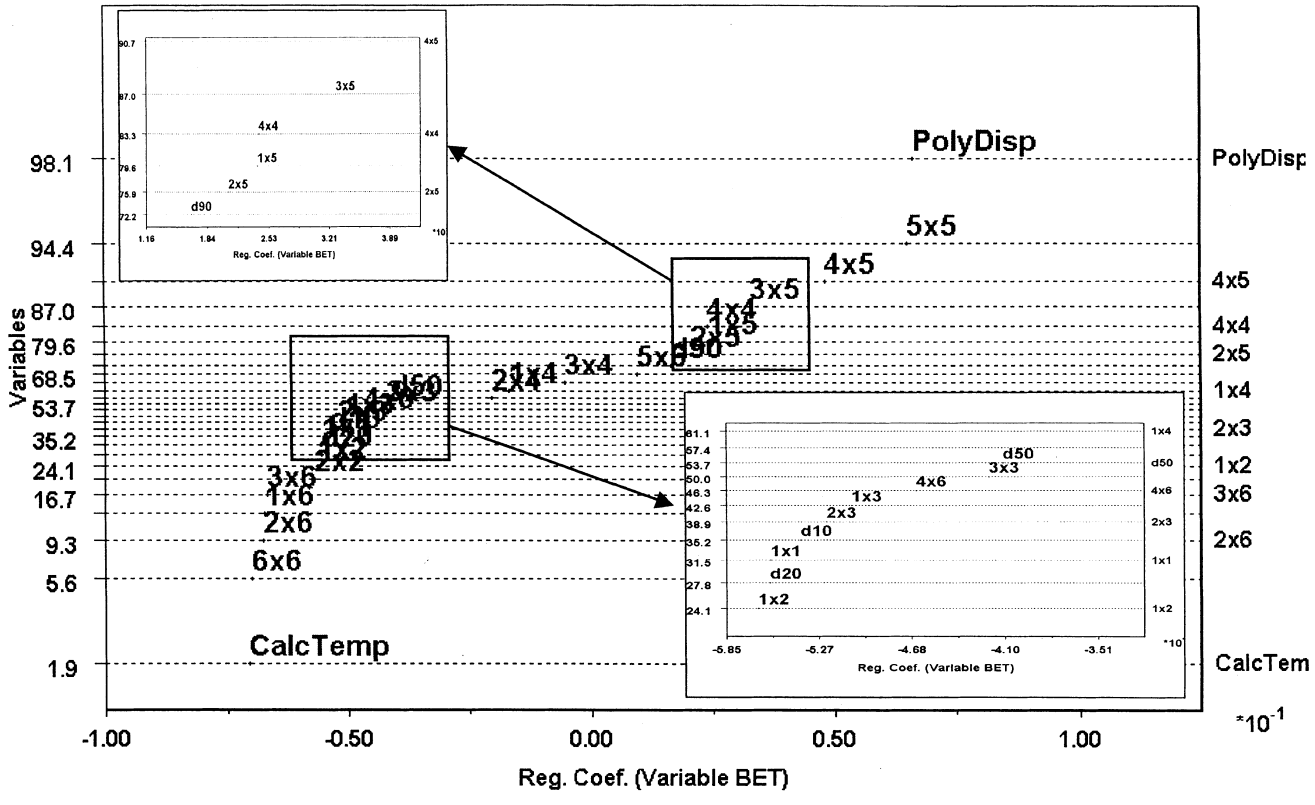

Fig. 14 Normal plot of the regression coefficients for model 3

models. Adding the cross-terms of the variables did not improve the models' predictive power. The best model to choose with regard to predictive power is therefore model 2.

Conclusions

PCS is a much faster method (approximately 10 min) for characterizing lanthanum chromite powders than BET surface area measurements (hours). Here we have shown that by the use of multivariate data analysis we can predict the BET surface area from the PLS model, based on the particle size distribution and the known calcination temperature. We are then able to save ourselves the more time consuming BET surface area measurements. In ceramic processing, where information about powder surface area and particle size is important for the packing efficiency and sinterability of the powder, use of multivariate data analysis techniques is highly recommended.

PCA gives the opportunity to easily reveal correlation among several variables at a time and to classify the powders.

Acknowledgements The authors would like to thank Jens Olav Sæten at Statoil Laboratories, Trondheim, Norway, for performing the BET surface area measurements. Gro Stakkestad is indebted to NFR (Norwegian Research Council) for financial support.

References

1. Minh NQ (1993) J Am Ceram Soc 76:563
2. Schafer W, Schmidberger R (1987) In: Vincenzini P (ed) High-tech ceramics. Elsevier P, Amsterdam, pp 1737–1742
3. Srilomsak S, Schilling DP, Anderson HU (1989) In: Singhal SC (ed) Proceedings of the 1st international symposium on solid oxide fuel cells. Electrochemical Society, Pennington, N.J., p 944
4. Armstrong TR, Stevenson JW, Pederson LR, Raney PE (1995) In: Dokiya M, Yamamoto O, Tagawa H, Singhal SC (eds) Proceedings of the 4th International Symposium on SOFC. Electrochemical Society proceedings series, vol 95-1. Electrochemical Society, Pennington, N.J., p 944
5. Hendriksen PV, Carter JD, Mogensen M (1995) In: Dokiya M, Yamamoto O, Tagawa H, Singhal SC (eds) Proceedings of the 4th International Symposium on SOFC. Electrochemical Society proceedings series, vol 95-1. Electrochemical Society, Pennington, N.J., p 934
6. Armstrong TR, Stevenson JW, Raney PE (1996) J Electrochem Soc 143:2919
7. Stakkestad G, Faaland S, Sigvartsen T (1996) Phase Transition 58:159
8. Faaland S, Stakkestad G, Bardal A, Sigvartsen T, Høier R (1996) In: Poulsen FW, Bonanos N, Linderoth S, Mogensen M, Zachau-Christiansen B (eds) Proceedings of the 17th Risö International Symposium on Materials Science. Risö National Laboratory, p 241
9. Lange FF (1989) J Am Ceram Soc 72:3
10. Pecora RJ (1964) Chem Phys 40:1604
11. Chu B (1974) Laser light scattering. Academic Press, New York
12. Ford NC (1985) In: Pecora R (ed) Dynamic light scattering. Plenum, New York, p 7
13. Ostrowsky N, Sornette D, Parker P, Pike ER (1981) Opt Acta 28:1059
14. Hulst HC (1957) Light scattering by small particles. Wiley, New York
15. Filella M, Zhang J, Newman ME, Buffle J (1997) Colloids Surf A 120:27
16. Wold S, Esbensen K, Geladi P (1987) Chemom Intell Lab Syst 2:37
17. Wold S, Albano C, Dunn W, Edlund U, Esbensen K, Geladi P, Hellberg S, Johanson E, Lindberg W, Sjöström M (1984) In: Kowalski BR (ed) Chemometrics: mathematics and statistics in chemistry. Reidel, Dordrecht, p 17
18. Martens H, Næs T (1991) Multivariate calibration. Wiley, Chichester
19. Manne R (1987) Chemom Intell Lab Syst 2:187
20. Shanefield DJ (1995) Organic additives and ceramic processing. Kluwer, Norwell, Mass
21. Brunauer S, Emmett PH, Teller E (1938) J Am Chem Soc 60:309
22. Gregg SJ, Sing KW (1967) Adsorbtion surface area and porosity. Academic Press, London
23. Dubinin MM (1960) Chem Rev 60:235
24. Shi JL, Lu CW, Kuo CL, Lin ZX, Yen TS (1992) Ceram Int 18:155
25. Ponthieu E, Grimblot J, Elaloui E, Pajonk GM (1993) J Mater Chem 3:287
26. Ismail HM, Hussein GAM (1996) Powder Technol 87:87
27. Zhang YS, Stangle GC (1994) J Mater Res 9:1997
28. Wurster DE, Oh E, Wang JCT (1995) J Pharm Sci 84:1301